Biomaterials 35 (2014) 970–982

Contents lists available at ScienceDirect

Biomaterials

journal homepage: www.elsevier.com/locate/biomaterials

The behavior of cardiac progenitor cells on macroporous pericardium-derived scaffolds

Sareh Rajabi-Zeleti [a,b], Sasan Jalili-Firoozinezhad [b], Mahnaz Azarnia [a], Fahimeh Khayyatan [b], Sadaf Vahdat [b], Saman Nikeghbalian [c], Ali Khademhosseini [d,e,f], Hossein Baharvand [b,g,*], Nasser Aghdami [b,**]

[a] Department of Biology, Kharazmi University, Tehran, Iran
[b] Department of Stem Cells and Developmental Biology at Cell Science Research Center, Royan Institute for Stem Cell Biology and Technology, ACECR, Tehran, Iran
[c] Shiraz Transplant Center, Namazi Hospital, Shiraz University of Medical Sciences, Iran
[d] Center for Biomedical Engineering, Department of Medicine, Brigham and Women's Hospital, Harvard Medical School, Boston, MA 02139, USA
[e] Harvard-MIT Division of Health Sciences and Technology, Massachusetts Institute of Technology, Cambridge, MA 02139, USA
[f] Wyss Institute for Biologically Inspired Engineering, Harvard University, Cambridge, MA 02139, USA
[g] Department of Developmental Biology, University of Science and Culture, ACECR, Tehran, Iran

ARTICLE INFO

Article history:
Received 11 October 2013
Accepted 15 October 2013
Available online 30 October 2013

Keywords:
Pericardium
Decellularization
Macroporous scaffold
Cardiac progenitor cells
Myocardial tissue engineering

ABSTRACT

Cardiovascular diseases hold the highest mortality rate among other illnesses which reveals the significance of current limitations in common therapies. Three-dimensional (3D) scaffolds have been utilized as potential therapies for treating heart failure following myocardial infarction (MI). In particular, native tissues have numerous properties that make them potentially useful scaffolding materials for recreating the native cardiac extracellular matrix (ECM). Here, we have developed a pericardium-derived scaffold that mimics the natural myocardial extracellular environment and investigated its properties for cardiac tissue engineering. Human pericardium membranes (PMs) were decellularized to yield 3D macroporous pericardium scaffolds (PSs) with well-defined architecture and interconnected pores. PSs enabled human Sca-1^+ cardiac progenitor cells (CPCs) to migrate, survive, proliferate and differentiate at higher rates compared with decellularized pericardium membranes (DPMs) and collagen scaffolds (COLs). Interestingly, histological examination of subcutaneous transplanted scaffolds after one month revealed low immunological response, enhanced angiogenesis and cardiomyocyte differentiation in PSs compared to DPMs and COLs. This research demonstrates the feasibility of fabricating 3D porous scaffolds from native ECMs and suggests the therapeutic potential of CPC-seeded PSs in the treatment of ischemic heart diseases.

1. Introduction

Cardiovascular diseases are the leading cause of death in industrialized nations and the developing world, account for approximately 40% of all human mortality [1]. A massive cardiomyocyte loss occurs following myocardial infarction (MI) which consequently leads to the development of non-contractible scar tissue [2]. Due to the shortage of organ donors and limited success of cell therapy, stem cell scientists, engineers and physicians continually seek new strategies for the regeneration of structural and functional features of an injured heart [3].

Myocardial tissue engineering is a promising approach that relies on combining appropriate cells with biomaterials to develop and create biological substitutes that resemble myocardium [4]. Although various natural and synthetic biomaterials have been employed within myocardial tissue engineering strategies, challenges remain in their ability to mimic the native extracellular matrix (ECM) microenvironment and effectively stimulate essential cellular responses [5–7]. Decellularized biological scaffolds, by transferring the appropriate signals to implanted cells, have the capability to support their retention, migration, proliferation and differentiation [8,9]. Upon decellularization, a significant amount of

* Corresponding author. Department of Stem Cells and Developmental Biology at Cell Science Research Center, Royan Institute for Stem Cell Biology and Technology, ACECR, PO Box 19395-4644, Tehran, Iran. Tel.: +98 21 22306485; fax: +98 21 23562507.
** Corresponding author.
E-mail addresses: Baharvand50@yahoo.com, Baharvand@royaninstitute.org (H. Baharvand), Nasser.Aghdami@royaninstitute.org (N. Aghdami).

0142-9612/$ – see front matter © 2013 Elsevier Ltd. All rights reserved.
http://dx.doi.org/10.1016/j.biomaterials.2013.10.045

immunogenic material would be removed, allowing the preserved ECM to orchestrate cell communications [10]. As a result, readily available natural platforms can be widely used as ideal candidates for regenerative medicine [11,12].

Due to the demonstrated benefits of decellularized organs for engineering other organs, the use of this approach may be advantageous for fabrication of myocardial patches [13,14]. Numerous decellularized scaffolds such as small intestine submucosa (SIS), urinary bladder and pericardium ECMs have been evaluated for use in ischemic myocardium treatment [15–17]. In this regard, pericardium membrane (PM) is an appropriate candidate for myocardial tissue engineering applications due to its biochemical and biomechanical properties that mimic the myocardial ECM [18]. Previous efforts at using PM as functional scaffolds have generated permeable constructs that enable cell migration with some challenges [19,20]. Recently, an injectable form of PM was proposed as a myocardial-engineered scaffold [21]. Despite many merits, a potential limitation of this approach was that the migration of cells within the gel was not improved compared to the collagen scaffolds (COLs). Additionally, the three-dimensional (3D) structure of the native tissue was lost during the fabrication process [21]. Several studies have shown that 3D macroporous scaffolds provide good physical, mechanical and structural support for proliferation and differentiation of seeded cells. It has been demonstrated that the interconnectivity of pores within such 3D structures enhances oxygen diffusion, nutrition transfer, cell migration and vascularization [22,23]. However, so far the use of 3D macroporous decellularized ECM scaffolds have not been broadly explored.

In this study, we aimed to fabricate a 3D macroporous cardiac patch that can mimic the myocardium ECM. It was anticipated that the 3D PM structure and mechanical properties would enhance desired cell–matrix interactions. In particular, to evaluate the synergistic effect of biological cues and the interconnected microstructure, we fabricated 3D macroporous PSs from human decellularized pericardium membranes (DPMs) by the freeze-drying method. We further evaluated the *in vitro* viability, migration, proliferation and differentiation of cardiac progenitor cells (CPCs) within these scaffolds. CPCs were used due to their ability to self-renew and differentiate into cardiomyocytes, fibroblasts, endothelial and smooth muscle cells. Furthermore, CPCs do not form teratomas [24,25] and improve heart function *in vivo* after being injected into the damaged myocardium following MI [26,27]. The placement of these cells in proper natural matrix may bring more promising outcomes in myocardial regeneration. Finally, we studied the potential of PSs to induce angiogenesis and direct the cardiac differentiation of CPCs compared to COLs and DPM *in vitro* and *in vivo* to test the suitability of this platform for myocardial treatment.

2. Materials and methods

2.1. Decellularization of PM

Human PM was provided by the Royan Tissue Department from cadavers and approved by the Ethical Committee for research applications. PM was maintained on ice while transported to the laboratory to prevent cellular lysis and damage to the matrix, then decellularized as previously described [21]. In brief, the sample was washed with Dulbecco's phosphate-buffered saline (PBS, Invitrogen, 21600-051) for 2 h and sodium dodecyl sulfate (SDS, Sigma L4390, 0.1% w/v) for 24 h, both in the presence of protease inhibitors. The tissue was finally treated with a nuclease solution (RNase/DNase), then washed in sterile PBS for 24 h by agitation, frozen overnight at −80 °C and lyophilized (Christ, Alpha 1-2 LD) for 24 h.

2.2. Scaffold fabrication

To fabricate PSs, decellularized pericardium was solubilized by enzymatic digestion using previously published protocols [21], after which the pericardium gel was fabricated. Briefly, fine milled pericardium powder (1.5% wt) was allowed to digest in pepsin (Merck, 107185) at 1 mg/ml that was dissolved in 0.1 M HCl for about 60 h under constant stirring. Afterwards, the solution was brought to pH 7.4 by the addition of 1 M NaOH and 10X PBS, which formed a viscous gel solution. Thereafter, solubilized ECM from the pericardium was poured into 24-well plates (TPP, Switzerland), frozen at −80 °C and lyophilized overnight.

DPM and COL were prepared for use as control materials. To fabricate DPMs, the decellularized pericardium was treated with 0.2 M acetic acid, followed by a wash with PBS, after which it was freeze-dried for 24 h in order to increase porosity within the structure. To fabricate COLs, collagen type I, extracted from rat tail by treatment with acetic acid, was dissolved at a 1% (w/v) concentration as previously described [28]. COLs were prepared according to the procedure mentioned for the PSs.

PS, DPM and COL were then chemically crosslinked for 24 h at 25 °C with a sterile solution of 50 mM 2-(N-morpholino) ethanesulfonic (MES, Sigma, M3671) in 70% ethanol (pH 5.4), 30 mM 1-ethyl-3-[3-dimethylaminopropyl] carbodiimide (EDC, Sigma, E7750) and N-hydroxysulfosuccinimide (NHS, Sigma Aldrich, 130672) at a molar ratio of 1:1. Following crosslinking, the scaffolds were thoroughly rinsed several times with double distilled water (d.d.H_2O) followed by three washes for 24 h with PBS, after which the samples were frozen at −80 °C and lyophilized until further use. The non-crosslinked samples of PS, DPM and COL were mentioned as N-PS, N-DPM and N-COL, respectively.

2.3. Evaluation of the decellularization process

2.3.1. Histological characterization

Native pericardium and DPM were fixed for 24 h in a 10% PBS/neutral buffered formalin solution (pH 7.4) at 25 °C. Subsequently, samples were washed in d.d.H_2O, dehydrated in a graded alcohol series, embedded in paraffin, and sectioned into 5 μm sections. The tissue slides were stained with hematoxylin and eosin (H&E, Sigma–Aldrich), Masson's trichrome (MT, Sigma–Aldrich), and alcian blue (AB, Sigma–Aldrich), after which they were assessed under a light microscope (BX51, Olympus). In addition, the tissue slides were stained with 4,6-diamidino-2-phenylindole (DAPI, Sigma–Aldrich, D8417) for confirmation of the absence of cell nuclei in the decellularized pericardium. Collagen and GAG contents were calculated for DPM relative to PM as fold change in intensity of green and blue hues in MT and AB histological sections, respectively. At least 100 fields were counted by three blinded investigators for each sample.

2.3.2. DNA quantification

Total DNA content was quantified in samples of native pericardium and DPM. Samples were completely homogenized and solubilized in 1 ml lysis buffer (50 mM tris-HCl, 50 mM EDTA, 1% SDS, 10 mM NaCl, pH 8.0) and subsequently digested in the presence of proteinase K, overnight in a water bath at 65 °C, followed by a phenol/chloroform extraction. DNA was precipitated from the aqueous phase with 100% ethanol, after which the extracts were subsequently washed with 70% ethanol. After dissolving the resultant pellet in RNase-free water, spectrophotometer was used to ascertain the concentration of DNA at 280 nm. The amount of DNA was averaged from a set of three independent runs and expressed as μg/mg dry weight of samples. For further examination, extracted DNA samples from both native and decellularized tissue were electrophoresed on 0.7% agarose gel in the presence of 1 μg/ml ethidium bromide (EthBr).

2.4. Physico-chemical characterization of scaffolds

2.4.1. Scanning electron microscope (SEM) analysis

Sample structure and morphology was analyzed with a scanning electron microscope (SEM, VEGA\TESCAN, Czech Republic) at an operating voltage of 15 kV. Samples were fixed in 2% glutaraldehyde in 0.1 M PBS and left for 24 h at 4 °C. After washing with 0.1 M PBS, the material was fixed in 1% OsO_4 in 0.1 M PBS (pH 7.3) for 2 h at 25 °C. Specimens were dehydrated in a graded ethanol-water series to 100% ethanol, then allowed to completely dry. Finally samples were mounted on aluminum stubs and coated with a thin layer of gold. We determined the average pore size by SEM after measuring the dimensions of at least 500 pores that were randomly chosen from the samples by Image Analyzer software (Image J 1.44p). The porosity of the scaffolds was calculated by determining the volume (V) and mass (m) of the scaffolds. Porosity of scaffolds was defined as:

$$\text{Porosity}(\%) = \left[1 - \frac{d_s}{d_p}\right] \times 100$$

where d_s and d_p are the density of the scaffold and average protein density (1.32 gr/cm^3), respectively [29,30].

For the cell-seeded samples, the scaffolds were fixed in 2% glutaraldehyde and subsequently processed for SEM examinations.

2.4.2. SDS-Page

Proteins were boiled with denaturing PAGE loading buffer (200 mM tris-HCl, 50% glycerol, 8% SDS, 400 mM DTT, 0.04% bromophenol blue, pH 6.8). One-dimensional gel electrophoresis was performed on pericardium solubilized ECM and compared with DPM and COL. The three solutions were run on 0.5 mM tris-HCl (pH 6.8), 8% polyacrylamide gel in tris/glycine/SDS buffer; a recombinant molecular weight marker (Sigma, M0671) was used as a standard protein. Samples were run

in a mini PROTEAN cell (Bio-Rad Laboratories, Hercules, CA) for 120 min at a constant of 15 mA/gel. Gels were fixed and stained according to a previously published protocol [31,32].

2.4.3. Collagen analysis

The collagen contents of PS, DPM and COL samples were quantified by using the SIRCOL Kit (Biocolor, United Kingdom) per the manufacturer's instructions. In brief, samples were thoroughly homogenized prior to solubilizing the collagen in a 0.1 M HCl-pepsin solution. After adding Sirius red dye to the samples, the absorbance at 555 nm was obtained and the collagen content of the samples determined against a standard curve of bovine collagen. The experiment was done in triplicate.

2.4.4. Glycosaminoglycan (GAG) quantification

To quantify the sulfated GAG contents of PSs, DPMs and COLs with the Blyscan GAG assay (Biocolor, United Kingdom), 30 mg of each sample digested in 1 ml of papain solution (Sigma, P3125) for 5 h at 65 °C. The tubes were occasionally vortexed. After centrifuging the sample aliquots, 1, 9-dimethyl-methylene blue dye was added to the pellets and absolute GAG levels were measured at 656 nm by extrapolating values from the standard curve of bovine tracheal chondroitin-4-sulfate (BRAND). Samples were run in triplicate.

2.4.5. Fourier transform infrared (FTIR) spectroscopy

Infrared spectra of non-crosslinked (N-COL and DPM) and EDC-crosslinked (COL and PS) samples were obtained using a Nexus 670 FTIR spectrometer (Nikolet, USA). Absorbance spectra were recorded at a resolution of 8 cm^{-1} in the range of 4000 to 500 cm^{-1}. Each spectrum was selected from a set of three samples and prepared independently under similar conditions. Data were analyzed by quantitative peak information.

2.4.6. Swelling measurements

The scaffold swelling behavior was determined at 37 °C in PBS (pH 7.4) for a defined time interval. The excess water in the scaffolds was blotted with a piece of filter paper and samples were weighed immediately on an electronic scale. The content of PBS in the swollen scaffolds was calculated as follows:

$$\text{Swelling ratio}(\%) = \left[\frac{(W_s - W_d)}{W_s}\right] \times 100$$

where W_s and W_d are the weights of the wet and dry scaffolds, respectively. The experiments were run in triplicate and averaged.

2.4.7. Degree of crosslinking

Crosslinking degree of the sponges was determined using the 2,4,6-trinitrobenzenesulfonic acid (TNBS) assay according to the following procedure. 5 mg samples were treated for 30 min with sodium bicarbonate solution (1 ml, 4% w/v). To this mixture, a freshly prepared TNBS solution (1 ml, 0.5% w/v) was added and the mixture incubated for 2 h at 40 °C. In order to hydrolyze the samples within 90 min, HCl (3 ml, 6 M) was added and the temperature increased to 60 °C. The resultant mixture was diluted with d.d.H_2O (5 ml) and cooled to 25 °C. A blank was prepared according to the above-mentioned procedure, by only the addition of TNBS solution after HCl. The absorbance of samples was correlated to degree of crosslinking according to the following equation:

$$\text{Degrees of crosslinking}(\%) = \left(1 - \frac{A_c}{A_n}\right) \times 100$$

where A_c and A_n are the absorbance of crosslinked and non-crosslinked samples, respectively. All the experiments were performed for five times.

2.5. Biomechanical characterization of scaffolds

Uniaxial compression and tensile tests were performed using a HCT-25/050 Zwick/Roell mechanical tester with a 50 N load cell at 25 °C. To measure compressive properties, lyophilized cylindrical specimens with 7.5 mm in diameter and 15 mm in height were used for testing. Samples of each composition were compressed as per ASTM standard and stress–strain data, compressive modulus (E), compressive strength (σ), maximum stress and load recorded at a crosshead speed of 1.3 mm/s with a strain level of 50%. The compressive modulus and compressive strength were determined as the slope of the linear region of the stress–strain curve corresponding with 0%–10% strain and the intersection point of two regression lines drawn from the collapse regime and linear elastic trend, respectively. In order to test the ultimate tensile strength (σ*) and Young's modulus (E*) of the scaffolds, uniaxial tension was exerted on samples until their failure. Samples in a dumb-bell shape with a gauge length of 10 mm and thickness of 1 mm were loaded at a tension speed of 5 mm/min. The tensile strength and modulus were obtained from stress–strain curves. The dimensions of all samples in both compressive and tensile tests were measured at four places in the samples by a digital electronic micrometer and averaged. All experiments were performed for five independent runs.

2.6. Cell culture studies

2.6.1. Culture of CPCs

CPCs were obtained from Royan Cell Bank Services with the appropriate informed consent for research use in addition to Ethical Committee approval. In brief, following obtaining heart biopsies during heart surgeries, transferring of ventricle septum tissue to laboratory and removing blood and probable contaminations, minced samples were incubated with an enzyme cocktail containing collagenase I (2 mg/ml) (Sigma, C0130), collagenase II (2 mg/ml) (Gibco, 17101-015), collagenase IV (1 mg/ml) and trypsin (2 mg/ml) (Gibco, 27250-018) at 37 °C. Thereafter, the enzyme was neutralized and cell suspensions were filtered and subsequently centrifuged. CPCs were then grown in proliferation culture medium, Iscoves modified Dulbecco's medium (IMDM, Sigma, 13390)/medium199 (M199, Gibco, 31150) at a 2:1 ratio with 1% L-glutamine (Invitrogen, 25030-032), penicillin/streptomycin (Invitrogen, 15140-122), 10% fetal bovine serum (FBS, Gibco, 10270-106) supplemented with 10 ng/ml basic fibroblast growth factor (bFGF, Royan Institute), 5 ng/ml epithelial growth factor (EGF, Invitrogen, PHG0315) and 5 ng/ml insulin-like growth factor-I (IGF-1, Sigma 13769) at 37 °C and 5% CO_2 in 95% humidity, according to a previous study [33]. The medium was changed every two days. After a one-week lag phase, cells became confluent. Cells were passaged with 0.025% trypsin/EDTA (Gibco, 15400) for 3 min at 37 °C.

2.6.2. Flow cytometry and fluorescence activated cell sorting

To determine cell surface marker distribution of the cells, flow cytometry analysis was used. Following candidate antibodies were utilized: CD117 (Miltenyi-Biotec, 130-091-734), CD105 (R&D Systems, FAB10971P), CD34 (BD, 550619), CD45 (Dako, F0861), Sca-1 (eBioscience, 12-5981-81), and CD31 (BD Pharmingen, 555445). For each marker 10^5 cells were treated with antibodies according to the manufacturer's instructions. Sca-1 surface antigen was used for purifying the cell population that was incubated with 10 μl of PE-conjugated anti-Sca-1 antibody per 10^6 cells for 30 min at 4 °C. Excess antibodies were removed by PBS, following centrifugation at 1500 rpm for 5 min. Subsequently the pellet was dissolved in sorting buffer [PBS^-, 1 mM EDTA (Sigma, ED4SS), 25 mM HEPES (Sigma, 90909c), 1% FBS, pH 7] and sorted by a FACSAria II™ instrument (BD, Becton Dickinson, USA), that was equipped with a 488 nm solid state blue laser. All flow cytometry data were analyzed by Flowing software (version 2.4, Turku Centre for Biotechnology) after six independent runs.

2.6.3. Cell culture on scaffolds

After sterilization, all scaffold groups were transferred into 24-well plates. A total of 5×10^5 cells/cm^2 were loaded on the scaffolds and cultured in proliferation culture medium for interested times. The medium was changed every two days. Because of the dense layer on each side of the DPM, this sample was sliced into 200 μm sections by a cryostat (LEICA, CM 1850) prior to cell seeding.

2.6.4. Histological and proliferation assessments

At seven days after the *in vitro* cell seeding, scaffolds were fixed for 24 h in 10% neutral buffered formalin solution in PBS (pH 7.4) at 25 °C. Subsequently, scaffolds were first washed with d.d.H_2O after which they were dehydrated in a graded alcohol series, embedded in paraffin and finally sectioned in 5 μm sections. Tissue slides were stained with H&E and MT. For immunostaining analysis, tissue slides were blocked with 10% goat serum and permeabilized with 1% Triton-X. Sections were then labeled with rabbit polyclonal primary antibody Ki67 (Abcam, ab66155) and incubated overnight at 4 °C. This procedure was performed according to immunostaining protocols with horseradish peroxidase–conjugated secondary antibody (Envision + System-HRP (DAB), Dako, k4011). Slides were counterstained with hematoxylin. Cells were observed under a light microscope (Olympus, BX51) and imaged with an Olympus DP72 digital camera that was mounted on the microscope. The images were studied by at least three blinded investigators.

2.6.5. Determination of cell metabolic activity

To determine the viability rate of Sca-1^+ CPCs within the scaffolds, the MTS (Promega, G5421) assay was performed according to the manufacturer's instructions. Briefly, Sca-1^+ CPCs were seeded on DPM, PS and COL at a density of 3×10^5 cells/cm^2 in 24-well tissue culture plates. The medium was changed every day. At days 3, 7 and 14, the scaffolds were transferred into new wells and the MTS solution was added to each well, after which the plates were incubated in the dark at 37 °C for 3 h. The absorbance of the solution was measured at 490 nm. The experiments were run in triplicate.

2.6.6. Evaluation of cell migration rate

For *in vitro* cell migration on day 7 tissue slides were de-paraffinized and hydrated in a graded alcohol series, after which they were stained with 1 μg/ml propidium iodide (PI, Sigma–Aldrich, P4170). The samples were visualized utilizing a fluorescent microscope (Olympus, BX51 with Olympus DP72 digital camera). The migration rate was assessed by measuring the depth of scaffold through which the fluorescent red cells penetrated and by counting the number of cells in consecutive layers of the scaffold. Migration index values were calculated as fold change in the number of cells per layer for DPM and PS relative to COL. At least ten slides were counted for each sample.

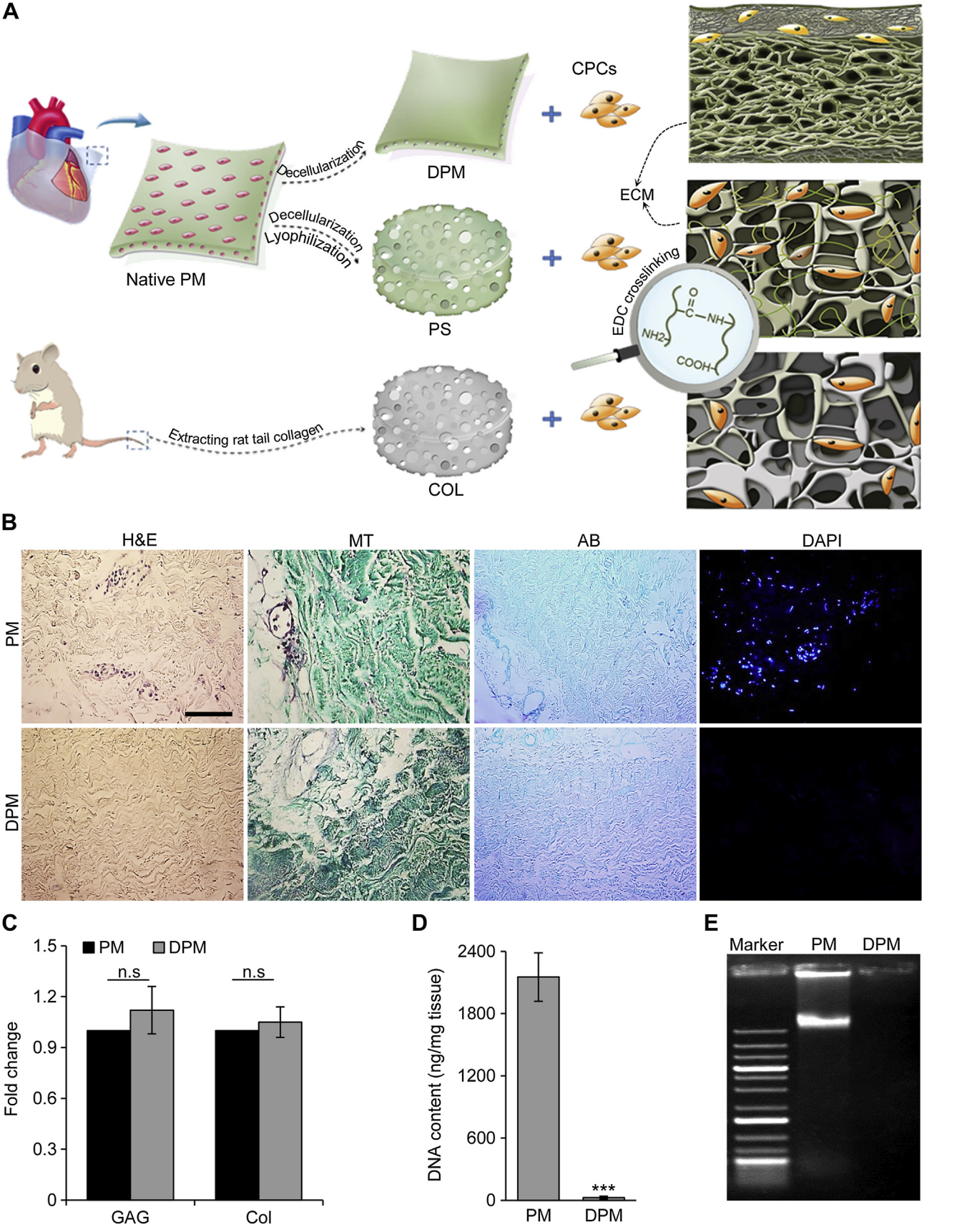

Fig. 1. Characterization of human DPM. (A) Schematic presentation of the fabrication procedure of three groups of scaffolds and subsequent cell seeding. (B) Histological analysis confirms the absence of nuclei and demonstrates the preservation of a DPM structure compared with native PM. (C) GAG and collagen quantification shows remaining of biochemical structure of DPM compared to PM. (n.s: not significant). (D) DNA quantification shows complete removal of DNA following mechanical and chemical treatments with significant differences in DNA content observed between PM and DPM, $n = 3$, ($^{***}P < 0.001$). (E) Gel electrophoresis shows DNA fragments of PM, whereas no DNA is observed in DPM. PM: Pericardium membrane, H&E: Hematoxylin and eosin, MT: Masson's trichrome, AB: Alcian blue, DAPI: 4′,6-diamidino-2-phenylindole. Scale bars: 200 μm.

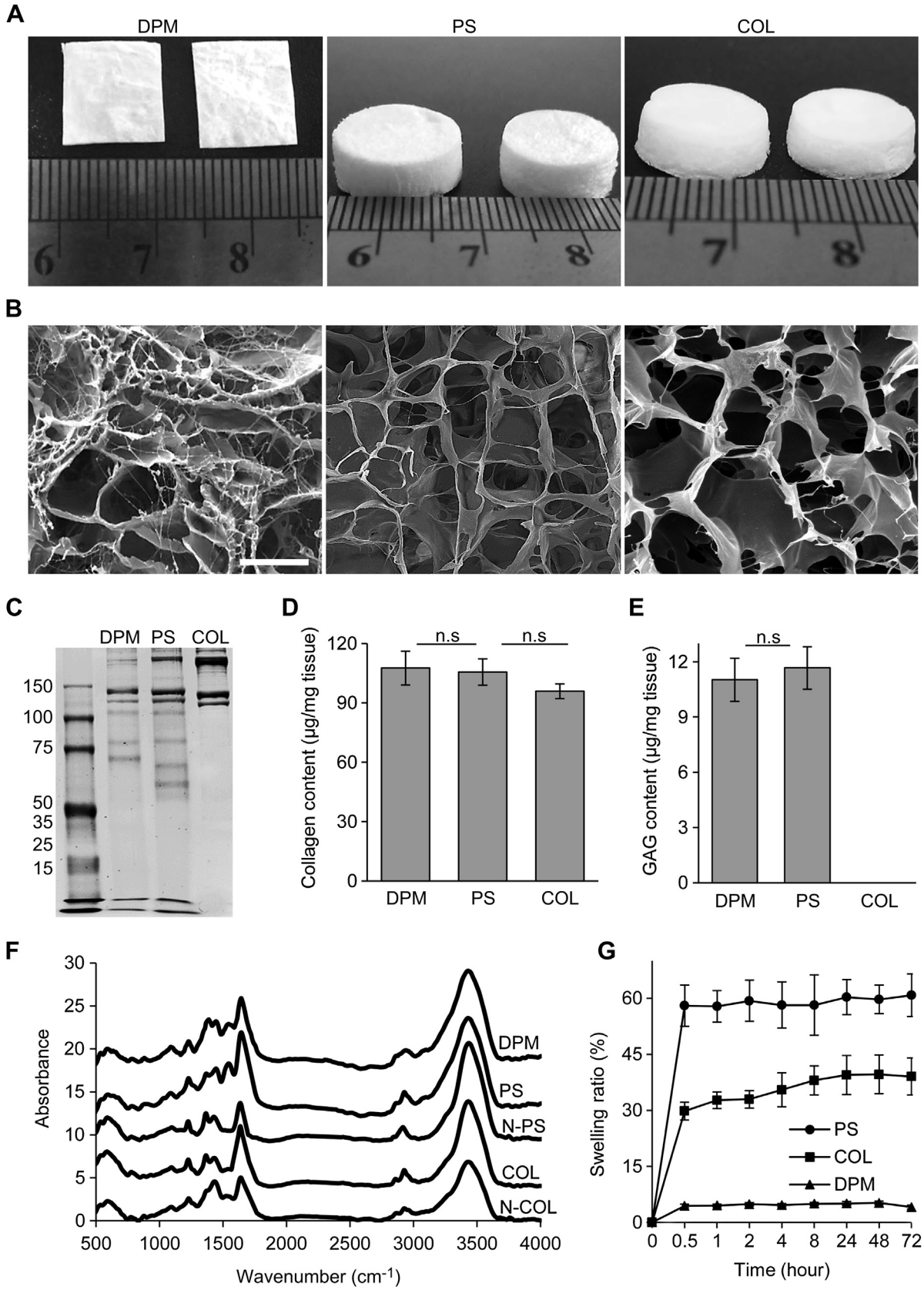

Fig. 2. Physicochemical characterization of the scaffolds. (A) Macroscopic images and (B) scanning electron micrographs of DPM, PS and COL prepared via the freeze-drying method. PS and COL show a homogenous macroscopic structure. (C) SDS-PAGE analysis shows increased complexity of the DPM and PS components compared to COL. (D) Collagen content demonstrates no significant difference between DPM and PS. (E) GAG quantity is almost similar in both the DPM and PS groups, while COL is devoid of GAGs. (F) FTIR spectra of N-COL, COL, N-PS, PS and DPM. (G) Swelling ratio of crosslinked scaffolds. PS shows the highest swelling ratio in comparison with other groups. $n = 3$, Scale bar: 50 μm (n.s: not significant).

2.6.7. RNA isolation and quantitative reverse transcriptase PCR (qRT-PCR)

RNA was extracted manually with TRIzol reagent (Ambion) and chloroform according to the manufacturer's instructions. First strand cDNA synthesis was performed with TaKaRa, PrimeScript 1st strand cDNA synthesis and Ex Taq kits according to their product datasheets. Gene expression was measured by quantitative real-time PCR for genes of interest. Reaction mixtures contained 10 μl of SYBR®Premix Ex Taq™ II (RR081Q, TaKaRa Bio, Inc.); 6 μl d.d.H_2O; 1 μl forward or reverse primers (5 pmol/μl); and 2 μl cDNA (50 ng/μl). PCR was performed on a Rotor-Gene™ 6000 Real-Time PCR System (Corbett Life Science) using the following program: 95 °C for 10 min (stage 1); 95 °C for 10 s, 60 °C for 20 s and 72 °C for 20 s, for 40 cycles (stage 2). Each sample was run in duplicate using three biologically independent replicates. The output data from Rotor-Gene 6000 analysis software (version 1.7, Corbett Life Science) were transferred to Microsoft Excel for further analysis. The results were normalized to GAPDH and expressed as fold change for DPM and PS relative to COL (ΔΔCt). Primer sequences are listed in Table S1.

2.7. In vivo study

All experiments in this study were performed in accordance with the guidelines established by the Committee on Animal Research at Royan Institute for Accreditation of Laboratory Animal Care. To evaluate the *in vivo* angiogenic and differentiation properties of the scaffolds, we used subcutaneous implantation. At three days prior to transplantation of the cell-loaded scaffolds, animals received cyclosporine (Novartis Pharma AG, Basel, Switzerland) with their drinking water [34]. Following a short-term general anesthesia, a small transverse incision was made on the backs of the rats followed by subcutaneous implantation of the DPMs, PSs and COLs into male Wistar rats that were 240–270 g in weight and 6–8 weeks old ($n = 3$ per group). After surgery, the rats were allowed to recover and permitted free access to water and food. Rats were sacrificed one month post-transplantation. Explants from each group were fixed in 10% formalin for histological assessment. Tissue slides were stained with H&E, MT and toluidine blue (TB, Sigma–Aldrich). In order to study the cellular events, at least three expert blinded investigators independently examined the stained tissue slides. Slides were graded according to four response degrees: fully covered area (F), partially covered area (P), group of cells (G) and individual cells (I). For better illustration, each cellular response pattern got a color and number value. The number of blood vessels was expressed as the average number of vessels per mm^2 of scaffolds (at least 20 slides were counted for each sample). To evaluate formation and maturation of blood vessels within scaffolds, immunohistochemistry analysis was performed for alpha-smooth muscle actin (α-SMA, Abcam, ab7817). The total area of SMA-positive blood vessels was expressed as a percentage of the total area of scaffold, as previously described (at least 100 cells were assessed for each scaffold). Immunohistochemistry for hTRA-1-85 (R&D, MAB3195) and α-MHC (Abcam, ab15) expression was performed to assess *in vivo* differentiation according to immunostaining protocols by using horseradish peroxidase–conjugated secondary antibody (LSAB + System-HRP, Dako K0679). The percentage of hTRA-1-85-positive cells and α-MHC positive cells was expressed as a percentage of the total cells (approximately 100 cells per sample were counted for each evaluation).

2.8. Statistical analysis

All data were expressed as mean ± standard deviation (SD). Statistical analysis for elucidation of differences in the measured properties between groups was accomplished using one-way analysis of variance (ANOVA) SPSS 16.0 software followed by Tukey's HSD post hoc test. *P* values of less than 0.05 were considered significant.

3. Results

3.1. Native macroporous scaffold fabrication strategy

In this study, we evaluated the ability of decellularized PSs to support the migration, proliferation and differentiation of CPCs.

Table 1
Compressive and tensile biomechanical properties of DPM, uncrosslinked and crosslinked PS and COL scaffolds.

Sample	Compression		Tension
	Max. stress (kPa)	σ (kPa)	σ[a] (kPa)
N-COL	2.2 ± 0.2[a]	1.4 ± 0.1	14.1 ± 1.7
COL	5.8 ± 0.4	5.4 ± 0.3	44.9 ± 4.4
N-PS	19.7 ± 2.1	8.1 ± 0.5	334.9 ± 16.6
PS	33.7 ± 4.3	10.5 ± 0.4	929.4 ± 46.4
N-DPM	N/D[b]	N/D	1845.5 ± 178.4
DPM	N/D	N/D	3016.7 ± 208.5

[a] Mean ± SD.
[b] N/D: not determined. The pericardium does not have a cylindrical shape in its native form.

Fig. 1A schematically represents the fabrication and seeding procedure of the three scaffold groups. Upon *in vitro* and *in vivo* investigations, CPCs were shown to penetrate and proliferate within PSs more than other control groups (Fig. 1A).

3.2. Decellularization of PMs

During decellularization, the PM turned white which indicated cell removal. In order to assess the effect of the decellularization process on ECM structure and components, histological analyses were performed. Histological findings from H&E and DAPI staining confirmed that the decellularization process was successful as there were no visible cell nuclei (Fig. 1B). As shown by MT and AB staining, the overall matrix histoarchitecture and major structural components, collagen and GAG, remained intact (Fig. 1B). In addition there did not appear to be a significant difference between PM and DPM in context of remaining GAG and collagen content of tissues (Fig. 1C). To determine the presence of decellularized tissue, DNA measurement was carried out and determined that approximately 99.9% of DNA was removed by the decellularization process in the DPM sample (20 ± 3 ng/mg) compared to native PM tissue (2153 ± 233 ng/mg; Fig. 1D). Extracted DNA samples from both native and decellularized tissue were negative for the presence of any DNA fragment on the agarose gel, which confirmed the previous result (Fig. 1E).

3.3. Physico-chemical characterization of scaffolds

To evaluate the microstructures of the scaffolds such as pore size, porosity and interconnectivity between the pores, SEM analysis was performed. SEM images revealed that the micro- and ultrastructural properties of the native PM were maintained after decellularization (Fig. 2B). The macrostructures of DPM, PS and COL are shown in Fig. 2A. The mean pore sizes of the scaffolds were: 82 ± 24 μm (DPM), 70 ± 12 μm (PS) and 81 ± 18 μm (COL). The porosity of the samples were approximately similar for all scaffolds, DPM (85.1%), PS (98.2%) and COL (99.2%).

To investigate the amount of proteins in the scaffolds, solubilized DPMs, PSs and COLs were assessed by SDS-PAGE. The collagen bands were identical in DPM and PS, however, the presence of a number of bands at lower molecular weights were also observed (Fig. 2C). Therefore, SDS-PAGE assessment showed additional ECM compartments or peptides, which showed the complexity of the pericardium tissue compared to COLs. There was no trace of enzymatic collagen degradation in the gel (Fig. 2C).

To assess the biochemical retention after scaffold fabrication, collagen and GAG analyses were performed. The collagen content was as follows: DPM (107.5 ± 8.5), PS (105.6 ± 6.7) and COL (95.9 ± 3.6) μg of collagen per mg of dry lyophilized weight (Fig. 2D). These results showed that the ECM composition was almost preserved after enzymatic digestion. GAG quantification assessment revealed that the decellularization treatment had no effect on the amount of this ECM component. The content of GAG in the DPMs and PSs was 11.1 ± 2.8 and 11.7 ± 4.9 μg GAG per mg of dry lyophilized weight, respectively, while no sulfated GAGs were present in the COL samples (Fig. 2E).

FTIR analysis was performed to evaluate the presence of any probable chemical alteration following the fabrication and crosslinking of the scaffolds. Fig. 2F shows the FTIR spectra of non-crosslinked (N-COL, N-PS) and EDC-crosslinked (COL, PS and DPM) scaffolds. By moving from non-crosslinked toward crosslinked scaffolds, diminution in carboxyl and amine-free groups bond (3417 cm^{-1}) in addition to symmetric stretching of the band of carboxylate salts bond (near 1420 cm^{-1}) were observed. The spectra also showed slight increases in the amide I bond

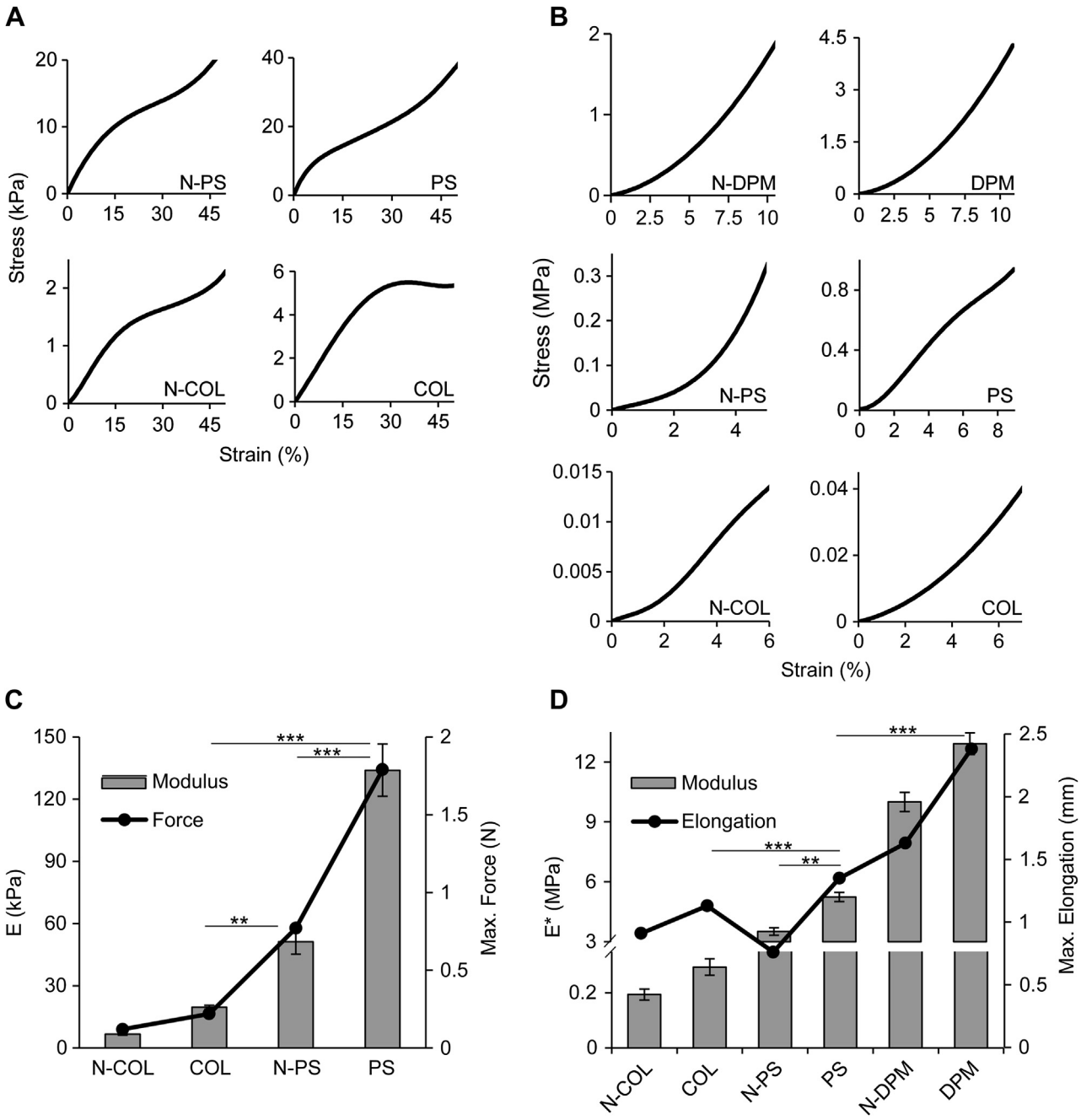

Fig. 3. Mechanical properties of uncrosslinked and crosslinked scaffolds. (A) Compressive strain-stress curves of fabricated scaffolds showing the complete curves of all samples. (B) Representative tensile stress–strain curves for various groups of scaffolds. (C) Compressive modulus [E] and maximum force for COL and PS samples before and after crosslinking. (D) Young's modulus (E^*) and maximum extension for DPM, N-COL, COL, N-PS, PS, N-DPM and DPM. $n = 3$, ($^{**}P < 0.01$, $^{***}P < 0.001$).

(1635 cm^{-1}). As a result of crosslinking, the spectra showed a significant increase in the ester bond (1072 cm^{-1}) from the N-PS to the PS. Spectra of all the samples also exhibited a peak at 2923 cm^{-1}, which was assigned to the stretching vibrations of the C–H bond.

Swelling behavior is of great importance in terms of the nutrition and waste transfer rate within the scaffolds. Swelling results of fabricated scaffolds were shown in Fig. 2G. The PSs had the highest ratio (approximately 60%) among the groups. COLs had approximately one-half, whereas DPMs showed approximately one-tenth of the water retention rate of PSs.

To assess the crosslinking efficiency, TNBS assay was performed. The extent of crosslinking is inversely proportional to the amount of free $-NH_2$ groups. The results showed a 75.3 ± 3.7%, 70.7 ± 2.9% and 72.4 ± 4.3% crosslinking of amino groups in the PSs, COLs and DPMs, respectively.

3.4. Mechanical characterization of scaffolds

Biomechanical tests were performed to estimate the adequacy of scaffold mechanical strength. Compressive strength, maximum compressive stress and load of non-crosslinked and crosslinked scaffolds are shown in Table 1 and Fig. 3A. The results showed that EDC crosslinking significantly increased maximum compressive stress by 2.7-fold in the COLs and 1.7-fold in the PSs. The

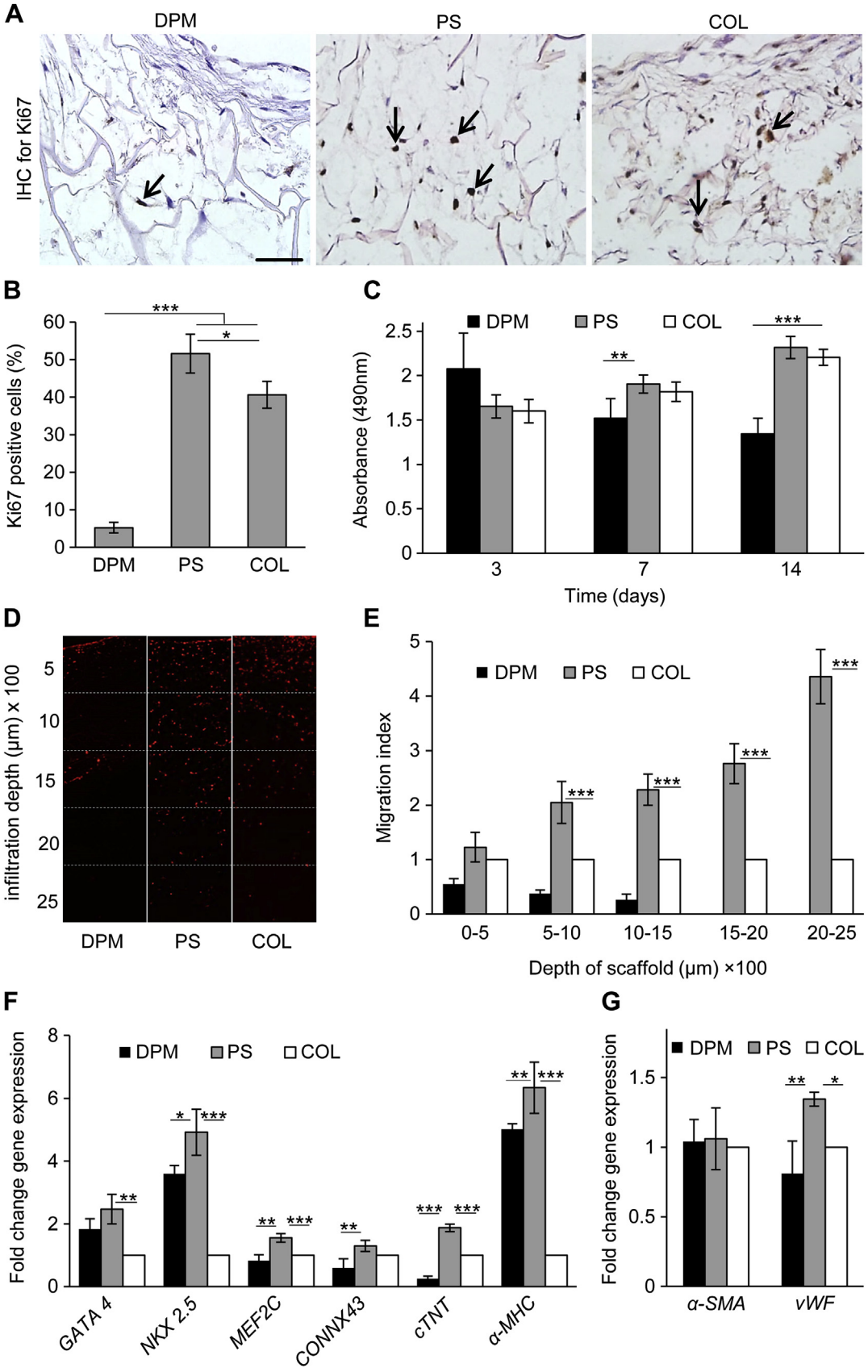

Fig. 4. *In vitro* evaluation of cell survival and proliferation into the scaffolds. (A) Cellular proliferation according to immunohistochemistry results for Ki67 on all scaffolds. Ki67 staining shows that the cells are in the active phase of the cell cycle (black arrow). (B) Quantitative analysis shows that the cells have the highest proliferation on PS ($n = 3$). (C) Metabolism and viability of CPCs seeded on scaffolds according to MTS analysis ($n = 3$). (D) PI staining of scaffolds on day 7 for evaluating cell migration through the scaffolds. (E) Comparative quantitative assessment of CPCs migration rate indicates that PS promotes infiltration ratio of cells through the scaffold. (F) Gene expression analysis for cardiac markers and (G) endothelial (vWF) and smooth muscle actin (SMA) markers on DPM and PS after seven days of culture ($n = 4–6$). The results are normalized to GAPDH and expressed as fold change for DPM and PS over COL (ΔΔCt). Scale bars: 50 μm, ($^{*}P < 0.05$, $^{**}P < 0.01$, and $^{***}P < 0.001$). Myocyte-specific enhancer factor 2C (*MEF2C*), cardiac troponin t (*cTNT*), myosin heavy chain (*α-MHC*), connexin 43 (*CONNX43*), glyceraldehyde 3-phosphate dehydrogenase (*GAPDH*): von Willebrand factor (*vWF*), and smooth muscle actin (*SMA*).

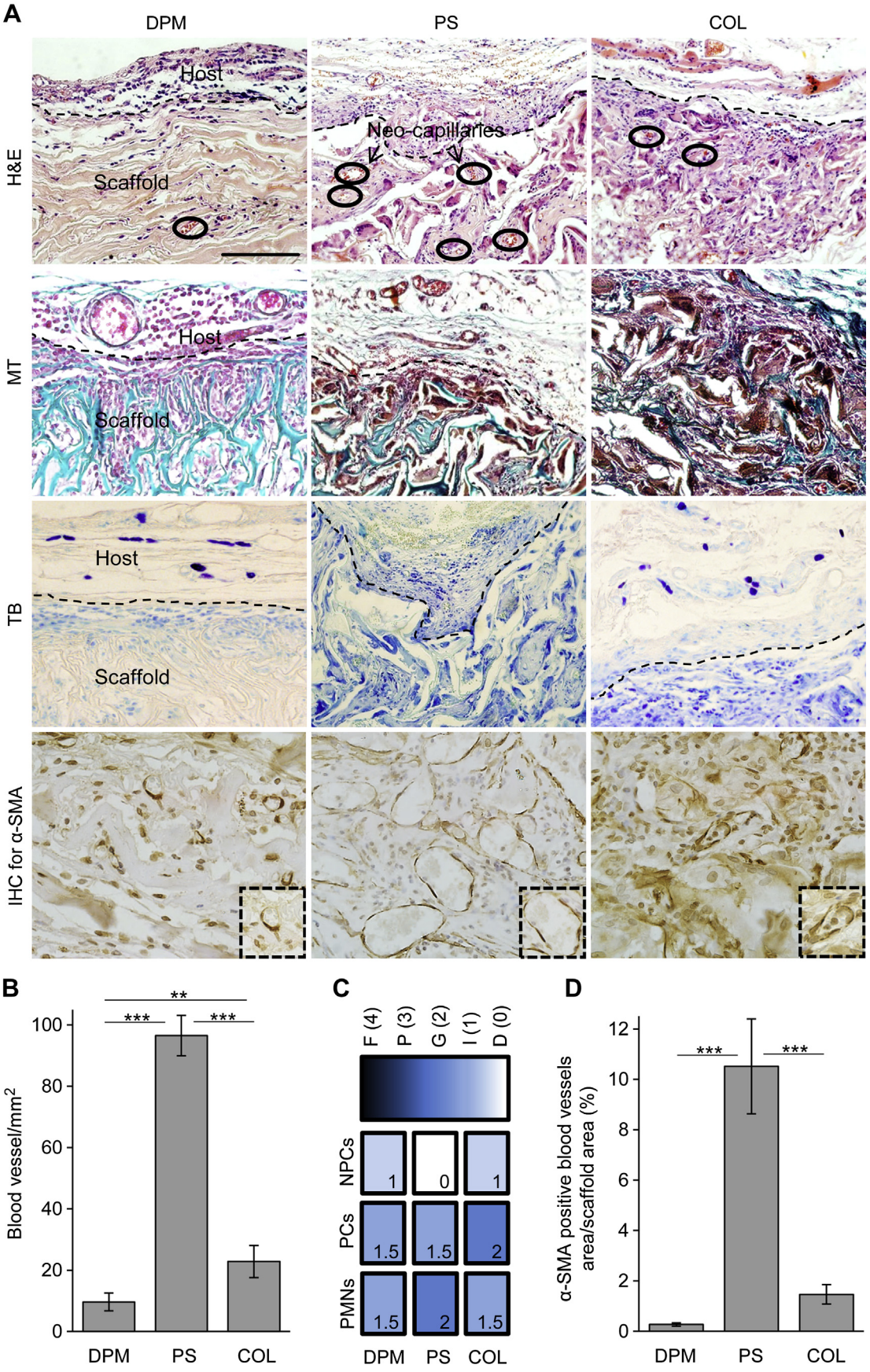

Fig. 5. Histological evaluation of explanted scaffolds on day 30 *in vivo*. (A) Hematoxylin and eosin (H&E) staining of DPM, PS and COL reveals the formation of neo-capillaries within the scaffolds (black circle). TB staining shows that while there are number of mast cells around the scaffolds, none went throughout the scaffolds. Immunohistochemistry for α-SMA

compressive strength of COLs was 5.4 kPa, whereas for PSs it was 10.5 kPa, which was significantly higher than N-COLs and COLs. As plotted in Fig. 3A, compressive stress–strain curves of the samples became non-linear at about 10% strain, after which furthered with collapse and densification regime. These three regions were completely shown for all scaffold groups. As shown in Fig. 3C, the compressive modulus (134.9 kPa) and maximum stress (1.8 N) of PSs increased compared with N-PS, which had a compressive modulus of 51.2 kPa and maximum stress of 0.8 N. In general, the overall compressive properties of PSs were almost one order of magnitude higher than the COLs.

The tensile properties of samples are also summarized in Table 1. In all cases, the maximum tensile strength and elongation increased with EDC crosslinking. The σ^* of PSs (929.4 kPa) was significantly higher than COLs (44.9 kPa). In the case of DPMs, this parameter increased tenfold (3016.7 kPa). Compared to N-PSs, the maximum elongation of the PSs enhanced by approximately two-fold (0.8 mm for N-PSs and 1.4 mm for PSs). Representative stress–strain curves for the five samples were roughly linear at almost 1% strain (Fig. 3B). Due to changes in origin and crosslinking of samples there were significant changes noted in the curves. As shown in Fig. 3D, while the elastic modulus of N-PS (3.5 MPa) and PS (5.2 MPa) samples were dramatically higher than the COL sample (0.3 MPa) they were significantly lower than the N-DPM (10.1 MPa) and DPM (12.9 MPa) samples.

3.5. Characterization of CPCs

We characterized the behavior of CPCs in culture prior to seeding to our scaffolds. In general we observed that after a week-long lag phase colonies appeared (Fig. S1A). Flow cytometry analysis of CPCs for CD117, CD105, CD34, CD45 and CD31 markers indicated that isolated cells were positive for CD105 (98.3 ± 2.3%), CD31 (15.1 ± 2.1%) and Sca-1 (17.9 ± 2.2%), however they were negative for CD34-45 (0.3 ± 1.1%) and CD117 (6.9 ± 1.2%; Fig. S1B). The isolated cells were sorted based on expression of Sca-1 surface marker to obtain a homogenous population of CPCs (Fig. S1C). The fraction of the Sca-1$^+$ cell content was approximately 92.5 ± 3.3% and the percentage of Sca-1$^+$ cells reached 98.9 ± 1.3% after three subsequent passages with other markers that included CD117 (0.7 ± 0.1%), CD105 (95.1 ± 2.1%), CD34-45 (0.03 ± 0.02%) and CD31 (0.2 ± 0.1%; Fig. S1D). RT-PCR was also used in order to assess gene expression profile of the cells in order to show their difference with cardiac fibroblasts. Expressions of several genes, included *abcg2* (stem cell marker), cardiac transcription factors such as *Nkx 2.5*, *GATA4*, *Tbx5* and *Mef2c*, and cardiac structural genes such as *α-MHC*, *β-MHC* and *Mlc-2v* were assessed. According to the data, expressions of cardiac structural genes were not observed in isolated cells (Table S2).

3.6. Evaluation of CPCs behavior on scaffolds

To investigate the interaction between CPCs and scaffolds, histological analyses were performed. Histological assessment of DPMs showed a dense structure with limited pore size and interconnectivity before treatment (Fig. 1B), which was confirmed by SEM micrographs (Fig. S2A). PM treatment with 0.2 M acetic acid was followed by lyophilization. A significant increase in the total porosity of DPMs was observed following acetic acid treatment (Fig. S2B–C). At seven days after CPCs seeding, H&E staining was performed in order to investigate the distribution of CPCs into the treated DPM. Cells were unable to infiltrate into the DPM due to the dense layer that was observed at the upper surface (Fig. S2D). When the upper dense layer was sliced off with a 200 μm cryostat microtome, there was a slight enhancement of penetration of CPCs into the depth of the treated DPMs (Figs. S2E, S3). In addition, the observed insignificant migration of CPCs through the acetic acid-treated lyophilized tissue was attributed to the lack of interconnectivity between pores (Figs. S2E, S3). In contrast, cell penetration was improved on scaffolds. The CPCs localization among the collagen fibers were examined by H&E and MT staining which revealed distribution of these fibers throughout the scaffold (Fig. S3). CPCs were localized both on the collagen fibers and in the pores. Cell morphology was also confirmed in all three groups by SEM analysis. SEM images showed strong affinity of the CPCs for the scaffolds (Fig. S3).

We also analyzed the proliferation of CPCs on the scaffolds through immunohistochemistry for Ki67 (Fig. 4A). While there was a significant population of Ki67-positive CPCs (at least $P < 0.05$) in the PSs (51.6 ± 5.2%), lower levels of expression were found in DPMs (5.2 ± 1.4%) and COLs (40.6 ± 3.6%) (Fig. 4B). In order to evaluate the effect of ECM on CPC viability and metabolic rate, cells were cultured on DPMs, PSs and COLs in the presence of proliferation medium after which the MTS assay was performed on days 3, 7 and 14. Results of the MTS assay demonstrated higher rates of cell proliferation related to PSs and COLs at days 7 and 14 compared to DPMs (Fig. 4C, $P < 0.01$).

To assess CPC migration through the scaffolds, PI staining was performed at on day 7. Cell infiltration into the PSs was significantly greater compared with COLs and DPMs (Fig. 4D). Owing to the lack of an interconnective structure in DPM, more than 80% of the cells were trapped in its upper layers and therefore attached to the top surface. As the depth of the scaffolds increased, the cellular infiltration percent in PSs was enhanced considerably compared to COLs and DPMs. As the migration index revealed, with the exception of the first steps of penetration, the numbers of cells in different depths of PSs were significantly higher than DPMs and COLs (Fig. 4E, at least $P < 0.001$). Overall, CPCs penetrated deeper into the PSs compared to other scaffold groups.

To assess the effect of ECM on CPC cardiogenic differentiation, quantitative real-time PCR was performed for genes *GATA-4, NKX 2.5, MEF 2c, Connxin 43*, α-myosin heavy chain (*α-MHC*), cardiac troponin T (*cTNT*), *vWF* and alpha smooth muscle actin (*α-SMA*). As shown in Fig. 4F, CPCs on DPMs and PSs showed increased expression of the early cardiac markers *GATA-4* (DPM:1.8 ± 0.3; PS: 2.5 ± 0.4), *NKX 2.5* (DPM: 3.6 ± 0.3; PS: 4.9 ± 1.1); *MEF2c* (DPM: 0.8 ± 0.2; PS:1.6 ± 0.1), *Connexin 43* (DPM: 0.6 ± 0.3, PS: 1.3 ± 0.2), *cTNT* (DPM: 0.3 ± 0.1, PS: 1.9 ± 0.1) and *α-MHC* (DPM: 5.1 ± 0.2; PS: 6.3 ± 0.8) compared with COLs. In addition, there was a significant increase in expression of the endothelial marker (vWF) in PSs (1.3 ± 0.1-fold) compared to DPMs (0.8 ± 0.2 fold). While there

showed the maturation rate of blood vessels within the scaffolds. (B) Quantification of vascular density within scaffolds during angiogenesis. Blood vessels density in the PS group was significantly higher than other groups one month after transplantation. (C) Wistar rat tissue response to the implanted scaffolds after one month was scored using a color scale (dark blue-whitish blue) and numbers (0–4), where fully cell covered areas are represented by more saturated tints and higher number values. (D) The total area of mature blood vessels (staining positive for α-SMA) per scaffold in PS was significantly more than other scaffolds. Scale bars: 100 μm, ($^{**}P < 0.01$, and $^{***}P < 0.001$). Alpha smooth muscle actin (α-SMA), PMNs: polymorphic nuclear cells (granulocytes), PCs: Phagocytic cells (macrophages and monocyte-derived giant cells), NPCs: Non-phagocytic cells (lymphocytes, plasma cells and mast cells), F: Fully cell covered, P: Partially cell covered, G: Group of cells, I: Individual cells, D: Devoid of cells. (For interpretation of the references to color in this figure legend, the reader is referred to the web version of this article.)

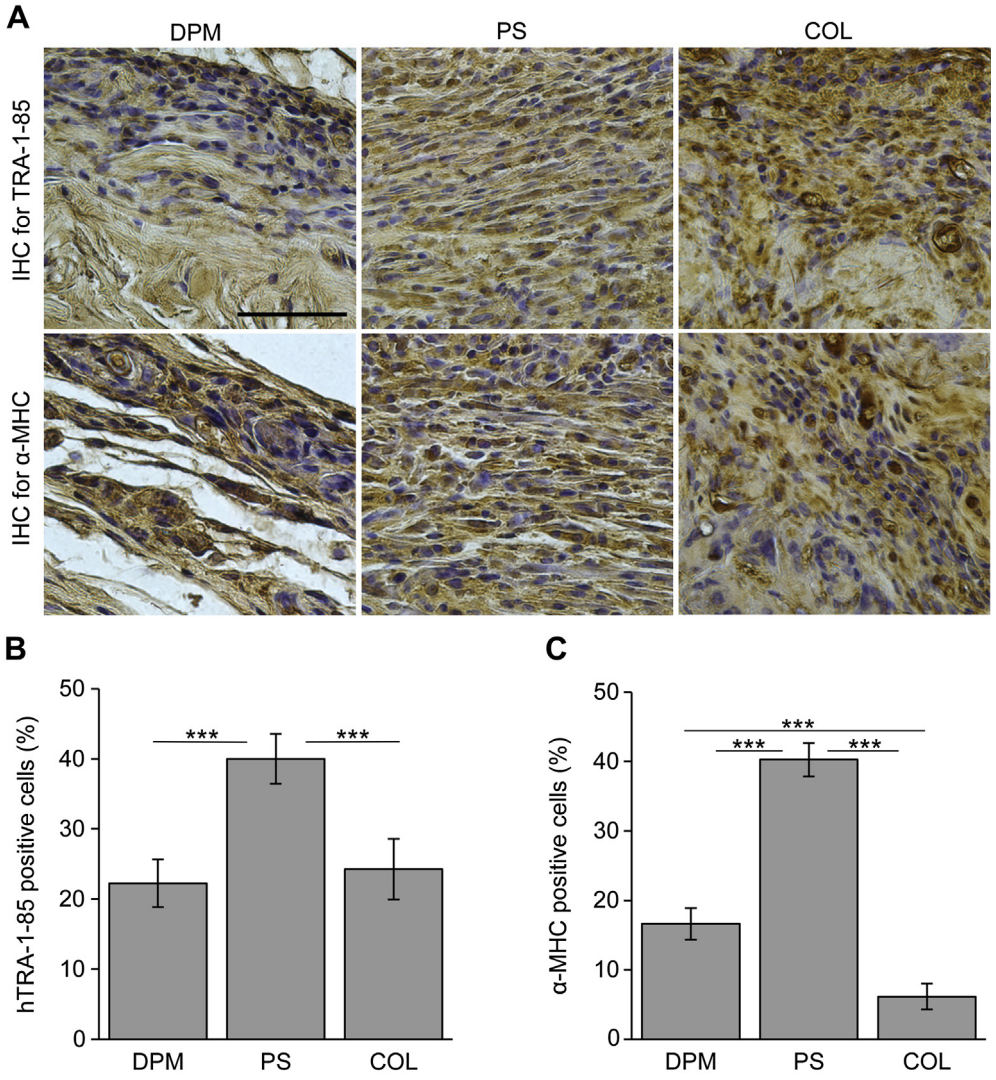

Fig. 6. Immunohistochemistry analysis of cell-seeded scaffolds *in vivo*. (A) Immunohistochemistry analysis of hTRA-1-85 and α-MHC staining of cells in the scaffolds one month post-transplantation in the rat model. (B) Quantitative analysis of hTRA-1 and (C) α-MHC positive cells showed increased numbers of cells in the PS group compared to the DPM and COL groups. Scale bars: 30 μm, ($^{***}P < 0.001$).

were no significant differences between groups in expression of smooth muscle actin marker (α-SMA) on day 7 (DPM: 1.1 ± 0.2 fold; PS: 1.1 ± 0.2 fold; Fig. 4G).

3.7. *In vivo* behavior of cellular infiltration and neovascularization

To evaluate the *in vivo* cellular response and assess the potential for samples to attract blood vessels, scaffolds were implanted subcutaneously in male rats. According to H&E staining there were a larger number of vessels in the PS group (Fig. 5A). Quantitatively, the PS group had the highest extent of neo-capillary formation (96.5 ± 6.5 blood vessels/mm^2, at least $P < 0.01$) throughout the scaffold at one month post-transplantation (Fig. 5B). Blood vessel distribution in both the DPM (9.6 ± 2.9 blood vessels/mm^2) and COL (22.8 ± 5.1 blood vessels/mm^2) groups were lower than amounts needed for tissue regeneration.

MT staining results showed mild fibrosis in the surrounding tissue of all scaffold groups (Fig. 5A). Moreover, new blood vessel formation was evident in supporting rat tissue. Scattered mast cells were evident in surrounding fibroadipose tissue on TB-stained slides in all three samples (Fig. 5A). Based on histological analyses with H&E, MT and TB staining, non-phagocytic cells (NPCs) were no longer observed in the PS. However there were moderate amounts of lymphocytes detected throughout the DPM and COL samples. Following one month *in vivo*, the COL group had evidence of larger amounts of macrophages and foreign body type giant cells compared to the PS and DPM groups. Moderate infiltration of granulocytes including polymorphonuclear (PMNs) and band cells were seen in DPMs, PSs and COLs. In addition, there was a capsular layer that surrounded all three groups of scaffolds (Fig. 5C).

Alpha-SMA-positively stained cells were detected in all groups (Fig 5A), however the size and percentage of mature vessels were highest in the PS group compared to the DPM and COL groups. As shown in Fig. 5D, PS showed a significantly higher α-SMA-positive blood vessel area per scaffold area (10.5 ± 1.9%) compared with DPM (0.27 ± 0.04%) and COL (1.5 ± 0.2%, $P < 0.001$).

3.8. *Differentiation assessment of CPCs in vivo*

To evaluate the *in vivo* fate of CPCs on subcutaneously transplanted scaffolds, immunohistochemistry analyses were performed for hTRA-1-85 to detect human cells and α-myosin heavy chain expression for differentiation assessment (Fig. 6A). As shown in Fig. 6B, hTRA-1-85 expression in PSs (40.2 ± 3.5%) was significantly

greater than DPMs (22.3 ± 3.4%) and COLs (24.3 ± 4.3%, $P < 0.001$). Our data also demonstrated that PSs had a strong effect on CPCs differentiation into myocytes (40.3 ± 2.4%) compared with DPM (16.6 ± 2.3%) and COLs (6.2 ± 1.9%, $P < 0.001$; Fig. 6C). Additionally, differentiated cells on PSs were aligned, morphologically organized and resembled myocytes compared with the other scaffolds.

4. Discussion

To promote repair of post-MI injuries and efficiently regenerate cardiac tissue, it is necessary to have an ideal scaffold that can provide proper physical and biochemical cues [3]. PM in the form of a sheet and gel has been shown to induce promising outcomes for cardiac repair [17,20]. Since human PM can be removed without detrimental effects and as it has a network of fibrous components that are composed of collagen, elastin and various GAGs, this biological scaffold is of considerable clinical interest.

Here we demonstrated the complete removal (>99%) of cellular contents through SDS decellularization protocol. By using this mild technique [9], native tissue components (GAGs and collagen) which play pivotal roles in original ECM construct [35] have been thoroughly preserved. In order to generate an interconnective PM platform, we generated a 3D macroporous scaffold from PM with hope of attaining better cellular responses. We obtained the desired mechanical strength of the scaffolds by utilizing a water soluble crosslinking agent, EDC [36]. Characterization of PSs showed that compared to native tissue, not only did the collagen content remain intact, but GAGs were also preserved after fabrication of the macroporous PSs. An increase in the ester bond of the PSs sample indicated that new crosslinks formed between GAG and collagen components, which proved the higher degree of crosslinking in this sample [37]. As confirmed by FTIR and TNBS data, the intensity of the functional groups and crosslink degree were more in the N-PS rather than the N-COL post-crosslinking. Because of the collagen and GAG content and pericardial microstructure, the crosslinking process had a significant impact on the mechanical properties of PSs compared to the COLs. Compressive and tensile moduli of PSs were more in the range of amounts reported in the literature for porous scaffolds intended for soft tissue engineering applications [38,39]. The compressive modulus of N-PSs and COLs was significantly lower than the native heart (approximately 400 kPa) [40]. Young's moduli of N-DPM and DPM were lower than the amounts reported for native human PM tissue (approximately 20 MPa) [41]. Former reports have postulated that this phenomenon is mainly due to the decellularization process [42,43]. Nevertheless, these values were more than the prospects of the current research goals [44]. The tensile strength value of PSs more closely approximated the reported amounts for synthetic cardiac scaffolds [45]. The stress–strain curves of samples in tensile and compressive tests resembled trend of human heart muscle and other reported myocardial scaffolds [39,45,46]. Biomechanical properties are not solely optimized by the presence of biological cues, in addition physical properties, cellular activities and angiogenesis are tuned by these native-like features [14]. Therefore, PSs can approximate the biophysical and biochemical features of myocardium ECM due to its pore size, material origin and degree of crosslinking.

The synergistic effect of pore interconnectivity and native biochemical signals resulted in a higher rate of CPC proliferation, metabolism and migration through the PS. The extent of proliferation, functionality, organization and differentiation of cells has been reported to be higher in 3D scaffolds [47]. The pore-related features and optimal swelling behavior of PSs regulate diffusion of nutrients, cellular behavior and vascular infiltration similar to other macroporous scaffolds [23].

The significant increase in expression of early cardiac markers within PSs compared to the control groups, confirmed the higher propensity of CPCs to become cardiomyocyte precursors at seven days after culture. Because the mature cardiac marker, *α-MHC*, was expressed in PSs at a greater level compared to the DPM and COL groups, in addition to the abundant amount of ECM found in myocardium post-infarction, it is possible that CPCs may represent better regeneration capacity in the macroporous PS sample. Furthermore, our *in vivo* results suggest that the macroporous pericardium scaffold, might provide a suitable microenvironment for differentiation of the implanted cells. This may be partially due to the biomechanical cues of our scaffolds [48].

Interestingly the substantial increase in endothelial gene expression *in vitro* was correlated with improved function and long-term survival of CPCs cultured in the PS. In this respect, the drawbacks of previous naturally derived cardiac ECMs improved by the advent of PSs [49]. In coordination with the *in vitro* results, the greater density of blood vessels in PSs after implantation in the rat model might increase the rate of oxygen and nutrient delivery, thus enhancing eventual regeneration of the intended region.

5. Conclusion

We successfully fabricated a 3D macroporous cardiac patch from human PM with biomimetic properties for myocardial tissue engineering. We have also demonstrated that the resulting macroporous scaffold enhances the proliferation, viability, migration and differentiation of CPCs *in vitro* compared to decellularized pericardium and collagen scaffolds. Angiogenesis and differentiation of the cells were augmented *in vivo* on pericardium 3D scaffold; we observed no immune rejection at one month after subcutaneous implantation. This study suggested that this macroporous pericardium-derived scaffold could serve as a clinically useful tissue engineered cardiac patch for the regeneration of a damaged heart following injury.

Competing financial interests

The authors declare they have no competing financial interests.

Acknowledgments

This study was supported by a grant from Royan Institute. The authors would like to express their appreciation to Dr. Niloufar Sodeifi, Shahab Mirshahvaladi, Pardis Khosravani, Keynoosh Khalooghi, Fatemeh Safari, and Forough Azam Sayahpour for their technical assistance and critical comments.

Appendix A. Supplementary data

Supplementary data related to this article can be found online at http://dx.doi.org/10.1016/j.biomaterials.2013.10.045.

References

[1] Roger VL, Go AS, Lloyd-Jones DM, Adams RJ, Berry JD, Brown TM, et al. Heart disease and stroke statistics-2011 update: a report from the American Heart Association. Circulation 2011;123:e18–209.
[2] Laflamme MA, Murry CE. Heart regeneration. Nature 2011;473:326–35.
[3] Vunjak-Novakovic G, Lui KO, Tandon N, Chien KR. Bioengineering heart muscle: a paradigm for regenerative medicine. Annu Rev Biomed Eng 2011;13:245–67.
[4] Tandon V, Zhang B, Radisic M, Murthy SK. Generation of tissue constructs for cardiovascular regenerative medicine: from cell procurement to scaffold design. Biotechnol Adv 2013;31:722–35.

[5] Karam JP, Muscari C, Montero-Menei CN. Combining adult stem cells and polymeric devices for tissue engineering in infarcted myocardium. Biomaterials 2012;33:5683–95.
[6] Callegari A, Bollini S, Iop L, Chiavegato A, Torregrossa G, Pozzobon M, et al. Neovascularization induced by porous collagen scaffold implanted on intact and cryoinjured rat hearts. Biomaterials 2007;28:5449–61.
[7] Bouten CV, Dankers PY, Driessen-Mol A, Pedron S, Brizard AM, Baaijens FP. Substrates for cardiovascular tissue engineering. Adv Drug Deliv Rev 2011;63:221–41.
[8] Yang B, Zhang Y, Zhou L, Sun Z, Zheng J, Chen Y, et al. Development of a porcine bladder acellular matrix with well-preserved extracellular bioactive factors for tissue engineering. Tissue Eng Part C Methods 2010;16:1201–11.
[9] DeQuach JA, Yuan SH, Goldstein LS, Christman KL. Decellularized porcine brain matrix for cell culture and tissue engineering scaffolds. Tissue Eng Part A 2011;17:2583–92.
[10] Bourgine PE, Pippenger BE, Todorov Jr A, Tchang L, Martin I. Tissue decellularization by activation of programmed cell death. Biomaterials 2013;34:6099–108.
[11] Badylak SF, Weiss DJ, Caplan A, Macchiarini P. Engineered whole organs and complex tissues. Lancet 2012;379:943–52.
[12] Mirmalek-Sani SH, Orlando G, McQuilling JP, Pareta R, Mack DL, Salvatori M, et al. Porcine pancreas extracellular matrix as a platform for endocrine pancreas bioengineering. Biomaterials 2013;34:5488–95.
[13] Ott HC, Matthiesen TS, Goh SK, Black LD, Kren SM, Netoff TI, et al. Perfusion-decellularized matrix: using nature's platform to engineer a bioartificial heart. Nat Med 2008;14:213–21.
[14] Badylak SF, Taylor D, Uygun K. Whole-organ tissue engineering: decellularization and recellularization of three-dimensional matrix scaffolds. Annu Rev Biomed Eng 2011;13:27–53.
[15] Okada M, Payne TR, Oshima H, Momoi N, Tobita K, Huard J. Differential efficacy of gels derived from small intestinal submucosa as an injectable biomaterial for myocardial infarct repair. Biomaterials 2010;31:7678–83.
[16] Robinson KA, Li J, Mathison M, Redkar A, Cui J, Chronos NA, et al. Extracellular matrix scaffold for cardiac repair. Circulation 2005;112:I135–43.
[17] Seif-Naraghi SB, Horn D, Schup-Magoffin PA, Madani MM, Christman KL. Patient-to-patient variability in autologous pericardial matrix scaffolds for cardiac repair. J Cardiovasc Transl Res 2011;4:545–56.
[18] Parker KK, Ingber DE. Extracellular matrix, mechanotransduction and structural hierarchies in heart tissue engineering. Philos Trans R Soc Lond B Biol Sci 2007;362:1267–79.
[19] Dong X, Wei X, Yi W, Gu C, Kang X, Liu Y, et al. RGD-modified acellular bovine pericardium as a bioprosthetic scaffold for tissue engineering. J Mater Sci Mater Med 2009;20:2327–36.
[20] Wei HJ, Chen SC, Chang Y, Hwang SM, Lin WW, Lai PH, et al. Porous acellular bovine pericardia seeded with mesenchymal stem cells as a patch to repair a myocardial defect in a syngeneic rat model. Biomaterials 2006;27:5409–19.
[21] Seif-Naraghi SB, Salvatore MA, Schup-Magoffin PJ, Hu DP, Christman KL. Design and characterization of an injectable pericardial matrix gel: a potentially autologous scaffold for cardiac tissue engineering. Tissue Eng Part A 2010;16:2017–27.
[22] Ma PX. Biomimetic materials for tissue engineering. Adv Drug Deliv Rev 2008;60:184–98.
[23] Rouwkema J, Rivron NC, van Blitterswijk CA. Vascularization in tissue engineering. Trends Biotechnol 2008;26:434–41.
[24] Wang X, Hu Q, Nakamura Y, Lee J, Zhang G, From AH, et al. The role of the sca-1+/CD31-cardiac progenitor cell population in postinfarction left ventricular remodeling. Stem Cells 2006;24:1779–88.
[25] van Vliet P, Roccio M, Smits AM, van Oorschot AA, Metz CH, van Veen TA, et al. Progenitor cells isolated from the human heart: a potential cell source for regenerative therapy. Neth Heart J 2008;16:163–9.
[26] Beltrami AP, Barlucchi L, Torella D, Baker M, Limana F, Chimenti S, et al. Adult cardiac stem cells are multipotent and support myocardial regeneration. Cell 2003;114:763–76.
[27] Linke A, Muller P, Nurzynska D, Casarsa C, Torella D, Nascimbene A, et al. Stem cells in the dog heart are self-renewing, clonogenic, and multipotent and regenerate infarcted myocardium, improving cardiac function. Proc Natl Acad Sci U S A 2005;102:8966–71.
[28] Rajan N, Habermehl J, Cote MF, Doillon CJ, Mantovani D. Preparation of ready-to-use, storable and reconstituted type I collagen from rat tail tendon for tissue engineering applications. Nat Protoc 2006;1:2753–8.
[29] Buttafoco L, Engbers-Buijtenhuijs P, Poot AA, Dijkstra PJ, Daamen WF, van Kuppevelt TH, et al. First steps towards tissue engineering of small-diameter blood vessels: preparation of flat scaffolds of collagen and elastin by means of freeze drying. J Biomed Mater Res B Appl Biomater 2006;77B:357–68.
[30] Fischer H, Polikarpov I, Craievich AF. Average protein density is a molecular-weight-dependent function. Protein Sci 2004;13:2825–8.
[31] Dyballa N, Metzger S. Fast and sensitive colloidal coomassie G-250 staining for proteins in polyacrylamide gels. J Vis Exp 2009;30.
[32] Dornish M, Kaplan D, Skaugrud O. Standards and guidelines for biopolymers in tissue-engineered medical products: ASTM alginate and chitosan standard guides. American Society for Testing and Materials. Ann N Y Acad Sci 2001;944:388–97.
[33] Smits AM, van Vliet P, Metz CH, Korfage T, Sluijter JP, Doevendans PA, et al. Human cardiomyocyte progenitor cells differentiate into functional mature cardiomyocytes: an in vitro model for studying human cardiac physiology and pathophysiology. Nat Protoc 2009;4:232–43.
[34] Pouya A, Satarian L, Kiani S, Javan M, Baharvand H. Human induced pluripotent stem cells differentiation into oligodendrocyte progenitors and transplantation in a rat model of optic chiasm demyelination. PLoS One 2011;6:e27925.
[35] Place ES, Evans ND, Stevens MM. Complexity in biomaterials for tissue engineering. Nat Mater 2009;8:457–70.
[36] Ma DH, Lai JY, Cheng HY, Tsai CC, Yeh LK. Carbodiimide cross-linked amniotic membranes for cultivation of limbal epithelial cells. Biomaterials 2010;31:6647–58.
[37] Calderon L, Collin E, Velasco-Bayon D, Murphy M, O'Halloran D, Pandit A. Type II collagen-hyaluronan hydrogel–a step towards a scaffold for intervertebral disc tissue engineering. Eur Cell Mater 2010;20:134–48.
[38] Ji C, Annabi N, Khademhosseini A, Dehghani F. Fabrication of porous chitosan scaffolds for soft tissue engineering using dense gas CO2. Acta Biomater 2011;7:1653–64.
[39] Annabi N, Mithieux SM, Zorlutuna P, Camci-Unal G, Weiss AS, Khademhosseini A. Engineered cell-laden human protein-based elastomer. Biomaterials 2013;34:5496–505.
[40] Dvir T, Timko BP, Brigham MD, Naik SR, Karajanagi SS, Levy O, et al. Nanowired three-dimensional cardiac patches. Nat Nanotechnol 2011;6:720–5.
[41] Lee JM, Boughner DR. Mechanical properties of human pericardium. Differences in viscoelastic response when compared with canine pericardium. Circ Res 1985;57:475–81.
[42] Mendoza-Novelo B, Avila EE, Cauich-Rodriguez JV, Jorge-Herrero E, Rojo FJ, Guinea GV, et al. Decellularization of pericardial tissue and its impact on tensile viscoelasticity and glycosaminoglycan content. Acta Biomater 2011;7:1241–8.
[43] Min BJ, Kim YJ, Choi JW, Choi SY, Kim SH, Lim HG. Histologic Characteristics and mechanical properties of bovine pericardium treated with decellularization and alpha-galactosidase: a comparative study. Korean J Thorac Cardiovasc Surg 2012;45:368–79.
[44] Venugopal JR, Prabhakaran MP, Mukherjee S, Ravichandran R, Dan K, Ramakrishna S. Biomaterial strategies for alleviation of myocardial infarction. J R Soc Interface 2012;9:1–19.
[45] Wang B, Tedder ME, Perez CE, Wang G, de Jongh Curry AL, To F, et al. Structural and biomechanical characterizations of porcine myocardial extracellular matrix. J Mater Sci Mater Med 2012;23:1835–47.
[46] Mathapati S, Bishi DK, Guhathakurta S, Cherian KM, Venugopal JR, Ramakrishna S, et al. Biomimetic acellular detoxified glutaraldehyde cross-linked bovine pericardium for tissue engineering. Mater Sci Eng C Mater Biol Appl 2013;33:1561–72.
[47] Kraehenbuehl TP, Langer R, Ferreira LS. Three-dimensional biomaterials for the study of human pluripotent stem cells. Nat Methods 2011;8:731–6.
[48] Engler AJ, Sen S, Sweeney HL, Discher DE. Matrix elasticity directs stem cell lineage specification. Cell 2006;126:677–89.
[49] French KM, Boopathy AV, DeQuach JA, Chingozha L, Lu H, Christman KL, et al. A naturally derived cardiac extracellular matrix enhances cardiac progenitor cell behavior in vitro. Acta Biomater 2012;8:4357–64.